Int. J. Heat Mass Transfer. Vol. 25, No. 2, pp. 243–253, 1982
Printed in Great Britain

0017–9310/82/020243–11 $03.00/0
Pergamon Press Ltd.

A NUMERICAL SOLUTION OF DEVELOPING TEMPERATURE FOR LAMINAR DEVELOPING FLOW IN ECCENTRIC ANNULAR DUCTS*

E. E. FELDMAN
Argonne National Laboratory, Argonne, IL 60439, U.S.A.

and

R. W. HORNBECK† and J. F. OSTERLE
Carnegie-Mellon University, Pittsburgh, PA 15213, U.S.A.

(*Received* 10 *September* 1980 *and in revised form* 21 *July* 1981)

Abstract—The energy equation expressed in bipolar coordinates is used to determine the temperature distribution in the thermal entrance region of an eccentric annular duct. An implicit alternating-direction method is used in the numerical solution. The analysis of the hydrodynamic entrance region, which provides the velocity distributions needed for the thermal solution, was obtained from a published solution by the present authors. A published Graetz solution for an eccentric annulus and a published combined thermal and hydrodynamic entrance region solution for the circular tube are used in the verification of the present solution. In the present analysis 17 combinations of fundamental thermal boundary conditions, Prandtl number, and annular geometry are considered. The annular geometry with equal relative eccentricity and radius ratio of 0.5 is used to study the effects of eccentricity and Prandtl number on the fluid temperature and surface heat flux distributions.

NOMENCLATURE

a, location of the positive pole of the bipolar coordinate system [m];
A, cross-sectional area of the duct, $\pi(r_{ow}^2 - r_{iw}^2)$ [m^2];
c, specific heat [J/(kg K)];
D_h, hydraulic diameter, $2(r_{ow} - r_{iw})$ [m];
e, absolute eccentricity, or center-to-center distance [m];
h, coordinate scale factor, defined by equation (9) [m];
H, dimensionless h, h/D_h;
k_f, fluid thermal conductivity [W/(m K)];
n, distance in normal direction [m];
Nu, local Nusselt number, defined by equation (35) and Table 2;
$\overline{Nu}$, Nu averaged around the complete circular arc of a duct wall at a fixed Z, defined by equations (38) and (39);
$\overline{\overline{Nu}}$, Nu averaged over the entire surface area of a wall from the inlet to a fixed Z, defined by equation (40);
Pr, Prandtl number, $\mu c/k_f$;
q'', local heat flux [W/m^2];
Q, volume rate of flow, $A\bar{w}$ [m^3/s];
r, radius [m];
Re, Reynolds number, $\rho\bar{w}D_h/\mu$;
t, time [s];
T, local temperature [K];
$\bar{T}$, mixed-mean average temperature, defined by equation (30) [K];
u, ζ component of velocity [m/s];
U, dimensionless u, $\rho uD_h/\mu$;
v, η component of velocity [m/s];
V, dimensionless v, $\rho vD_h/\mu$;
w, axial component of velocity [m/s];
$\bar{w}$, average w (volume rate of flow per unit area) [m/s];
W, dimensionless w, $w/\bar{w}$;
x,y, Cartesian coordinates in the transverse plane [m];
z, axial coordinate [m];
Z, dimensionless z, $(z - z_e)/(D_hRe)$.

Greek symbols

γ, radius ratio, r_{iw}/r_{ow};
ΔZ, dimensionless axial step size;
ε, relative eccentricity, $e/(r_{ow} - r_{iw})$;
ζ,η, bipolar coordinates in the annular cross-section;
θ, dimensionless T, defined by Table 1;
$\bar{\theta}$, dimensionless $\bar{T}$, defined by equation (32);
μ, coefficient of viscosity [Pa.s];
ρ, density [kg/m^3];
Φ, dimensionless q'', defined by equations (21) and (22);
$\bar{\Phi}$, Φ averaged around the complete circular arc of a duct wall at a fixed Z, analogous to $\overline{Nu}$ of equations (38) and (39);
Ω, circumferential arc length measured along either wall (a value of 0° corresponds to the widest point of the annular gap and a value of 180° corresponds to the narrowest point).

* Research performed at Carnegie-Mellon University, Pittsburgh, Pennsylvania.
† Deceased.

Subscripts

e, entrance (inlet to the duct);
i,j, indices which together denote points of the finite difference grid (i corresponds to ζ and j to η);
iw, inner wall;
ow, outer wall;
max, maximum.

1. INTRODUCTION

WHEN A confined flow with fully developed velocity and temperature profiles experiences a step change in thermal boundary condition, the resultant thermal entry region problem is known as the Graetz problem. Hatton and Quarmby [1] and Lundberg *et al.* [2] analyzed the laminar flow Graetz problem for concentric annuli. Vilenskii *et al.* [3] consider only heat flux boundary conditions in their numerical solution of the Graetz problem for laminar flow in eccentric annuli. Cheng and Hwang [4] and Trombetta [5] obtained infinite series approximations for the fully developed temperature distributions for laminar flow in eccentric annuli.

When heat transfer from the walls of a duct begins at the inlet to the duct, both velocity and temperature profiles develop simultaneously. Murakawa [6] and Heaton *et al.* [7] analyzed this combined thermal and hydrodynamic entrance region problem for laminar flow in concentric annuli. Shumway and McEligot [8] numerically solved both the Graetz problem and the combined entrance region problem for laminar flow with variable properties in concentric annuli.

The basis for the present analysis is Feldman [9] which provides the only known solution to the combined entrance region problem for laminar flow in eccentric annuli. Feldman *et al.* [10] provides the hydrodynamic entrance region solution which is used in the present solution of the thermal entrance region.

2. MATHEMATICAL MODEL

The fluid is assumed to be incompressible, laminar, Newtonian, and to have constant properties. Body forces, viscous generation of heat and axial heat conduction are neglected. Since the steepest axial temperature gradients generally occur at the inlet, the error introduced by excluding axial conduction is expected to decrease with increasing distance from the inlet. Moreover, accurate results can not be expected if the Peclet number (product of Reynolds number and Prandtl number) is less than 50. Some of the many investigations concerning axial heat conduction in laminar duct flow are discussed in [11]. Thus only forced convection is analyzed and the governing energy equation in vector form is

$$\frac{DT}{Dt} = \frac{k_f}{\rho c}\nabla^2 T \tag{1}$$

where t is time, ρ is density, k_f is thermal conductivity, T is temperature, and c is specific heat.

The bipolar coordinates used in [10] in the representation of the hydrodynamic model are also used in the representation of the energy equation, equation (1). The bipolar coordinates (ζ,η) are related to the Cartesian coordinates (x,y) by the following two equations.

$$\left(\frac{x}{a}\right)^2 + \left(\frac{y}{a} - \coth\zeta\right)^2 = \operatorname{csch}^2\zeta \text{ for } -\infty < \zeta < \infty \tag{2}$$

$$\left(\frac{x}{a} - \cot\eta\right)^2 + \left(\frac{y}{a}\right)^2 = \csc^2\eta \text{ for } 0 \le \eta \le 2\pi \tag{3}$$

Figure 1 shows curves of constant ζ and constant η plotted as functions of x and y.

The geometry of any eccentric annulus can be characterized by the radius ratio, γ, and the relative eccentricity, ε, which are given by

$$\gamma = \frac{r_{iw}}{r_{ow}}, \tag{4}$$

$$\varepsilon = \frac{e}{r_{ow} - r_{iw}}, \tag{5}$$

where the subscripts iw and ow correspond to the inner and outer wall of the annulus, respectively, r is the wall radius, and e is the absolute eccentricity, or center-to-center distance, of the annulus. As explained in [10]

$$\cosh\zeta_{ow} = \frac{\gamma(1-\varepsilon^3) + (1+\varepsilon^2)}{2\varepsilon} \tag{6}$$

$$\cosh\zeta_{iw} = \frac{\gamma(1+\varepsilon^2) + (1-\varepsilon^2)}{2\varepsilon\gamma}. \tag{7}$$

These two equations and planar symmetry confine the region of interest to $(\zeta_{ow} \le \zeta \le \zeta_{iw},\ 0 \le \eta \le \pi)$.

The general orthogonal curvilinear coordinate expressions for the vector operations of equation (1) along with the necessary bipolar coordinate scale factors can be found in [12]. In the bipolar coordinate representation of equation (1), the second derivative of temperature with respect to the axial coordinate, z, is not included because axial heat condition is assumed to be negligible. Hence the energy equation may be written as

$$\frac{u}{h}\frac{\partial T}{\partial \zeta} + \frac{v}{h}\frac{\partial T}{\partial \eta} + w\frac{\partial T}{\partial z} = \frac{k_f}{\rho c}\frac{1}{h^2}\left[\frac{\partial^2 T}{\partial \zeta^2} + \frac{\partial^2 T}{\partial \eta^2}\right], \tag{8}$$

where u, v and w respectively are the ζ, η and z components of fluid velocity, h is a bipolar coordinate

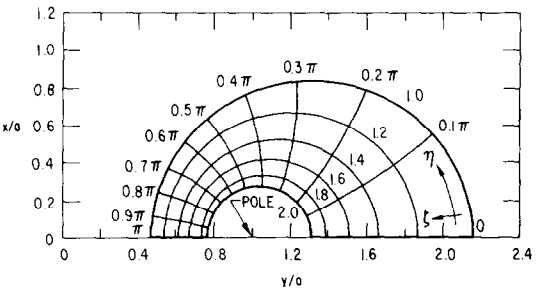

FIG. 1. Bipolar coordinate curves for the region $(1.0 \le \zeta \le 2.0,\ 0 \le \eta \le \pi)$.

Table 1. Dimensionless temperature and boundary conditions

Fundamental solution	Case	Dimensionless temperature*	Boundary conditions Outer wall	Inner wall
First kind	1A	$\theta = \dfrac{T - T_e}{T_{ow} - T_e}$	$\theta = 1$	$\theta = 0$
	1B	$\theta = \dfrac{T - T_e}{T_{iw} - T_e}$	$\theta = 0$	$\theta = 1$
Second kind	2A	$\theta = \dfrac{k}{q''_{ow} D_h}(T - T_e)$	$\Phi_{ow} = 1$	$\Phi_{iw} = 0$
	2B	$\theta = \dfrac{k}{q''_{iw} D_h}(T - T_e)$	$\Phi_{ow} = 0$	$\Phi_{iw} = 1$
Third kind	3A	$\theta = \dfrac{T - T_e}{T_{ow} - T_e}$	$\theta = 1$	$\Phi_{iw} = 0$
	3B	$\theta = \dfrac{T - T_e}{T_{iw} - T_e}$	$\Phi_{ow} = 0$	$\theta = 1$
Fourth kind	4A	$\theta = \dfrac{k}{q''_{ow} D_h}(T - T_e)$	$\Phi_{ow} = 1$	$\theta = 0$
	4B	$\theta = \dfrac{k}{q''_{ow} D_h}(T - T_e)$	$\theta = 0$	$\Phi_{iw} = 1$

*The subscripts e, ow, and iw refer to the entrance to the duct, the outer surface and inner surface, respectively.

scale factor, given by

$$h = \frac{a}{\cosh \zeta - \cos \eta} \tag{9}$$

and a is the location of the pole (see Fig. 1).

Before equation (8) can be solved, thermal boundary conditions must be specified. Although any combination of temperature and heat flux distributions may be imposed at the walls, in order to produce results of general utility, we will assume that at each wall of the duct either the temperature or the heat flux is uniform. Because the energy equation is homogeneous and linear in temperature, temperature solutions may be superimposed. Reynolds *et al.* [13] have taken the principle of superposition into consideration in defining four fundamental solutions corresponding to four pairs of thermal boundary conditions. For each solution, the inlet temperature distribution is uniform. The four fundamental kinds of solutions have the following boundary conditions:

First kind—one wall is at the constant temperature of the entering fluid, while the other is at a different constant temperature;

Second kind—one wall has a uniform heat flux, while the other is insulated;

Third kind—one wall is at a constant temperature different from the inlet temperature, while the other wall is insulated;

Fourth kind—one wall has a uniform heat flux, while the other is at the inlet temperature;

The heat flux, q'', at either wall according to Fourier's law, is

$$q'' = -k_f \frac{\partial T}{\partial n}, \tag{10}$$

where n is the direction normal to the wall and the direction of positive q''. The required temperature gradient in bipolar coordinates is

$$\frac{\partial T}{\partial n} = \frac{1}{h}\frac{\partial T}{\partial \zeta}. \tag{11}$$

It is convenient to define q'' to be positive when it causes heat to flow into the fluid. Thus, the heat flux into the fluid at the inner wall will be in the negative ζ direction and the two wall heat fluxes are

$$q''_{ow} = -k_f \left(\frac{1}{h}\frac{\partial T}{\partial \zeta}\right)_{ow}, \tag{12}$$

$$q''_{iw} = +k_f \left(\frac{1}{h}\frac{\partial T}{\partial \zeta}\right)_{iw}. \tag{13}$$

3. METHOD OF SOLUTION

Equation (8) and the boundary conditions are expressed in dimensionless form with u, v, w, z and h, respectively, represented by

$$U = \frac{\rho u D_h}{\mu}, \tag{14}$$

$$V = \frac{\rho v D_h}{\mu}, \tag{15}$$

$$W = \frac{w}{\bar{w}}, \tag{16}$$

$$Z = \frac{z - z_e}{D_h Re}, \tag{17}$$

$$H = \frac{h}{D_h}, \tag{18}$$

where μ is the coefficient of viscosity, $\bar{w}$ is the average axial velocity, i.e. volumetric flow divided by the cross-sectional area, z_e is the value of z corresponding to the duct inlet, and D_h and Re are the hydraulic diameter and the Reynolds number respectively given by

$$D_h = 2(r_{ow} - r_{iw}) = 2a(1 - \gamma)\,\mathrm{csch}\,\zeta_{ow}, \tag{19}$$

$$RE = \frac{\rho \bar{w} D_h}{\mu}. \tag{20}$$

Table 1 provides the definition of dimensionless temperature, θ, and the boundary conditions for each of the four fundamental solutions. In accord with equations (12) and (13), the dimensionless heat flux at the outer and inner walls are:

$$\Phi_{ow} = -\left(\frac{1}{h}\frac{\partial\theta}{\partial\zeta}\right)_{ow}, \tag{21}$$

$$\Phi_{iw} = +\left(\frac{1}{h}\frac{\partial\theta}{\partial\zeta}\right)_{iw}. \tag{22}$$

In all cases listed in Table 1, θ equals 0 at the inlet, and θ or Φ equals 1.0 at the heated wall and 0 at the unheated wall.

The dimensionless form of equation (8) is

$$Pr\left(\frac{U}{H}\frac{\partial\theta}{\partial\zeta} + \frac{V}{H}\frac{\partial\theta}{\partial\eta} + W\frac{\partial\theta}{\partial z}\right) = \frac{1}{H^2}\left(\frac{\partial^2\theta}{\partial\zeta^2} + \frac{\partial^2\theta}{\partial\eta^2}\right) \tag{23}$$

where Pr is the Prandtl number and is given by

$$Pr = \frac{\mu c}{k_f}. \tag{24}$$

By combining equations (9), (18), and (19), one can express the dimensionless scale factor, H, as

$$H = \frac{0.5 \sinh \zeta_{ow}}{(1 - \gamma)(\cosh \zeta - \cos \eta)}. \tag{25}$$

A finite difference solution for equation (23) is obtained from a numerical marching technique in which the thermal entrance region is sectioned into a series of parallel planes perpendicular to the Z axis. The thermal solution at the first plane beyond the inlet is obtained independently of all succeeding planes. The solution for the second plane depends only upon that for the first and, similarly, the solution for the $k + 1$ plane depends only upon that for its immediate predecessor, the k plane. Thus, the entire thermal entrance region is solved by solving one plane at a time in succession.

In each plane, the region ($\zeta_{ow} \le \zeta \le \zeta_{iw}, 0 \le \eta \le \pi$) is sectioned by sets of constant ζ curves (with index i) and constant η curves (with index j) to form a finite difference grid covering half of the symmetric annular cross-section. This grid is the same one used by [10] to solve the hydrodynamic model and obtain values of U, V, and W at each grid point of each Z plane. While the grid has 24 equal η intervals, the 32 ζ intervals are generally unequal with very fine intervals near the two walls where large velocity and temperature gradients occur. Hence, there are 775, i.e. $(32 - 1)\cdot(24 + 1)$, interior grid points for which values of $\theta_{i,j}$ are required and 25 points on each ζ boundary for which $\theta_{i,j}$ is governed by the boundary conditions given in Table 1.

At each Z plane the values of $U_{i,j}$, $V_{i,j}$ and $W_{i,j}$ were obtained for each of the 775 interior points from the hydrodynamic solution presented by [10] and are used in the numerical approximation to equation (23), which is represented at each of these 775 grid points. The values of θ beyond $0 \le \eta \le \pi$ which are needed for the η derivatives at $\eta = 0$ and $\eta = \pi$ are obtained from symmetry conditions at these two values of η. At each set of 25 points along $\zeta = \zeta_{ow}$ and $\zeta = \zeta_{iw}$, the boundary conditions provided in Table 1 are represented. For the constant temperature boundary conditions, this representation is either $\theta = 0$ or $\theta = 1.0$, and for the constant heat flux boundary conditions, the numerical approximation to $\partial\theta/\partial\zeta$ is set equal to $+H$ or to $-H$. Hence, in all cases at each Z plane there are 825 equations and an equal number of unknown values of $\theta_{i,j}$.

An implicit alternating-direction method [14] was used in the numerical solution of the energy equation. This solution method uncouples the groups of algebraic equations which result from the finite difference representation of equation (23). In the solution at the first plane beyond the inlet, the η derivatives are implicitly represented by unknown values of $\theta_{i,j}$ in the solution plane, while the ζ derivatives are evaluated with the known uniform $\theta = 0$ temperature distribution at the inlet. In the solution at the second plane beyond the inlet, the alternate arrangement is used with the ζ derivatives implicitly represented in the solution plane while the η derivatives are evaluated with known $\theta_{i,j}$ values of the first plane. This alternating two-step cycle is repeated until the entire thermal entrance region has been solved.

At the planes where the η derivatives are expressed implicitly, the algebraic equations corresponding to points along a curve of constant η are independent of those for all other values of η. The analogous situation prevails at the planes where the ζ derivatives are expressed implicitly. This method is advantageous because it is much easier to solve a series of independent groups of simultaneous equations than it is to solve the same total number of equations as one simultaneous set. Since each independent group of simultaneous equations can be represented by a tridiagonal matrix, a simple direct method of solution (see [14]) can be used.

The finite difference approximations of the ζ, η and Z derivatives of equation (23) are analogous to their counterparts used by [10] for the momentum equation. The axial derivative in the $k + 1$ plane is a simple 1st-order backward difference involving values of θ in both the $k + 1$ and k planes. The two η

derivatives were grouped together and approximated by a finite difference approximation provided by Allen [15]. Similarly, the two ζ derivatives were grouped together and approximated by the extension of Allen's method provided by [10] for unequally spaced grids. When the first derivative is not present, Allen's method produces the familiar central-difference representation of the second derivative, which can be obtained from a 2nd-order Taylor series approximation.

The heat flux boundary conditions require that $\partial\theta/\partial\zeta$ be approximated at ζ_{ow} and ζ_{iw}. Since all of the ζ intervals in the finite difference grid occur in pairs of equal size, a 2nd-order Taylor series approximation for equally spaced grids can be used. Hence, at the outer wall where ζ_{ow} corresponds to the grid index $i = 1$,

$$\left(\frac{\partial\theta}{\partial\zeta}\right)_{i,j} \approx -\frac{3\theta_{1,j} - 4\theta_{2,j} + \theta_{3,j}}{2\,\Delta\zeta_1}, \tag{26}$$

and at the inner wall where ζ_{iw} corresponds to $i = N + 1$,

$$\left(\frac{\partial\theta}{\partial\zeta}\right)_{N+1,j} \approx \frac{3\theta_{N+1,j} - 4\theta_{N,j} + \theta_{N-1,j}}{2\Delta\zeta_N}, \tag{27}$$

where $\Delta\zeta_1$ and $\Delta\zeta_N$ are the sizes of the first and last ζ interval, respectively.

In the Graetz problem, the velocity profile is fully developed and only the temperature profile is developing. Hence, for this problem, equation (23) can be reduced to

$$H^2 W \frac{\partial\theta}{\partial Z'} = \frac{\partial^2\theta}{\partial\zeta^2} + \frac{\partial^2\theta}{\partial\eta^2}, \tag{28}$$

where

$$Z' = Z/Pr. \tag{29}$$

In equation (28), W corresponds to the fully developed flow solution and Pr does not appear.

The average mixed-mean temperature, $\bar{T}$, at any axial plane for constant density is defined as

$$\bar{T} = \frac{\int_A Tw\,dA}{Q}, \tag{30}$$

where A is the flow area and Q is the volumetric flow rate. By definition, Q is the product of A and the average axial velocity, $\bar{w}$. When equation (30) is expressed in bipolar coordinates, the result can be written as

$$\bar{T} = \frac{2}{\pi(r_{ow}^2 - r_{iw}^2)\bar{w}} \int_0^{\pi} \int_{\zeta_{ow}}^{\zeta_{iw}} Tw^2\,d\zeta\,d\eta, \tag{31}$$

or in dimensionless form as

$$\bar{\theta} = \frac{8}{\pi}\,\frac{1-\gamma}{1+\gamma} \int_0^{\pi} \int_{\zeta_{ow}}^{\zeta_{iw}} \theta W H^2\,d\zeta\,d\eta, \tag{32}$$

where $\bar{\theta}$, the dimensionless average temperature, corresponds to θ in Table 1 when $\bar{T}$ replaces T. Since there are an even number of equal η intervals and all of the ζ intervals are in pairs of equal size, the double-integral in equation (32) is approximated with the aid of Simpson's 1/3 rule.

Since, for boundary conditions of the second kind, the heat flux at each wall is specified, $\bar{\theta}$ can be directly calculated from energy considerations. Hence, in this special case

$$\bar{\theta}_{2A} = \frac{4}{1+\gamma}\,(Z/Pr), \tag{33}$$

$$\bar{\theta}_{2B} = \frac{4\gamma}{1+\gamma}\,(Z/Pr), \tag{34}$$

where the subscripts 2A and 2B correspond to Cases 2A and 2B of Table 1.

The local Nusselt number, Nu, which at either wall can vary both circumferentially as well as axially, is defined as

$$Nu = \frac{h_f D_h}{k_f} \tag{35}$$

where the film coefficient, h_f, is given by

$$h_f = \frac{q_w''}{T_w - \bar{T}}, \tag{36}$$

and T_w is the local temperature at the wall and q_w'' is q_{ow}'' or q_{iw}'' as given by either equation (12) or (13). Equations (35) and (36) yield

$$Nu = \frac{D_h}{k_f}\,\frac{q_w''}{T_w - \bar{T}}, \tag{37}$$

The definitions of θ given in Table 1 and equations (12), (13), (21), (22), and (37) yield the Nu relationships given in Table 2.

Table 2. Local Nusselt number

Fundamental solution	Case*	Outer wall	Inner wall
First kind	1A	$\dfrac{\Phi_{ow}}{1-\bar{\theta}}$	$-\dfrac{\Phi_{iw}}{\bar{\theta}}$
	1B	$-\dfrac{\Phi_{ow}}{\bar{\theta}}$	$\dfrac{\Phi_{iw}}{1-\bar{\theta}}$
Second kind	2A	$\dfrac{1}{\theta-\bar{\theta}}$	0
	2B	0	$\dfrac{1}{\theta-\bar{\theta}}$
Third kind	3A	$\dfrac{\Phi_{ow}}{1-\bar{\theta}}$	0
	3B	0	$\dfrac{\Phi_{iw}}{1-\bar{\theta}}$
Fourth kind	4A	$\dfrac{1}{\theta-\bar{\theta}}$	$-\dfrac{\Phi_{iw}}{\bar{\theta}}$
	4B	$-\dfrac{\Phi_{ow}}{\bar{\theta}}$	$\dfrac{1}{\theta-\bar{\theta}}$

* See Table 1.

At any given axial location the Nusselt number distribution around either wall may be integrated from $\eta = 0$ to $\eta = \pi$ and then divided by the included arc length to obtain the circumferentially averaged Nusselt number, $\overline{Nu}$. For the outer and inner walls, respectively, the two $\overline{Nu}$ relationships, expressed in bipolar coordinates, are

$$\overline{Nu}_{ow} = \frac{2(1-\gamma)}{\pi} \int_0^{\pi} (Nu\, H)_{ow}\, d\eta, \tag{38}$$

$$\overline{Nu}_{iw} = \frac{2(1-\gamma)}{\pi\gamma} \int_0^{\pi} (Nu\, H)_{iw}\, d\eta. \tag{39}$$

In the analysis, the above two integrals are approximated with the aid of Simpson's 1/3 rule.

A local Nusselt number distribution can also be integrated over the wall surface area from $Z = 0$ to $Z = Z$. When this result is divided by the wall surface area, a surface-averaged Nusselt number, $\overline{\overline{Nu}}$, is obtained. This quantity can also be obtained by integrating $\overline{Nu}$ from $Z = 0$ to $Z = Z$ and dividing the result by Z. Hence, for either wall

$$\overline{\overline{Nu}} = \frac{1}{Z} \int_0^{Z} \overline{Nu}\, dZ. \tag{40}$$

The integral in this equation is numerically approximated by

$$\int_0^{Z} \overline{Nu}\, dZ \approx \int_0^{Z-\Delta Z} \overline{Nu}\, dZ + (\overline{Nu})_Z \Delta Z, \tag{41}$$

where ΔZ is the size of the last axial step taken to reach Z.

Because the finite difference solution employs numerical approximations whose truncation errors approach zero as the axial step sizes approach zero, some initial experimentation was necessary to ensure that sufficiently small step sizes were chosen. Extremely small values of ΔZ are used near the duct inlet where steep axial gradients of temperature and flow occur. In some of the hydrodynamic solutions of [10], a ΔZ of 0.25×10^{-5} at the duct inlet was gradually increased to 0.001. Although these step sizes are quite adequate for the hydrodynamic solution, they cause a local oscillation in the temperature solutions. In some instances this numerical instability was extremely severe. Empirically obtained stability criteria, used by Torrance [16] in the numerical solution of 2-dim. transient natural convection in an enclosure, suggested the following criterion on ΔZ:

$$\Delta Z \leq \min \left\{ \frac{Pr\, H^2 W}{\dfrac{2}{(\Delta\zeta)^2} + \dfrac{2}{(\Delta\eta)^2}} \right\} \tag{42}$$

where the minimum is taken over all interior grid points, and $\Delta\zeta$ and $\Delta\eta$ are the local interval sizes of the finite difference grid. Although the above criterion eliminated the numerical instability, the indicated ΔZ is of the order of 10^{-9}. Fortunately, the need for an excessively large number of axial steps was avoided since stable thermal solutions were obtained by gradually increasing the 10^{-9} inlet value of ΔZ to 0.001 as Z increased.

Fully developed temperature distributions were obtained by solving the Graetz problem for a sufficiently large Z/Pr. A typical Graetz solution required 2100 axial steps (1050 two-step cycles) to obtain a thermal solution at $Z/Pr = 1.56$. This solution required about $4\frac{1}{2}$ minutes of computing time on the Univac 1108 computer at the Carnegie-Mellon University Computation Center. Additional details concerning the Graetz and combined entrance region solutions, along with the FORTRAN IV computer programs used to generate them, can be found in [9].

4. RESULTS

The present solution for developing flow with $Pr = 1.0$ is compared with that of Hornbeck [17] for the circular tube. Although for all values of ε the annular geometry approaches that of the tube as γ approaches zero, the highly eccentric geometry ($\varepsilon = 0.9, \gamma = 0.1$) was chosen in order to produce a severe test of both the present thermal model and the hydrodynamic model of [10]. Contrary to the assumptions used in a similar comparison presented in [9], in this paper the dimensionless variables of the tube and the annulus are defined in an analogous manner, with the hydraulic diameter for the tube being its diameter and the hydraulic diameter of the annulus being given by equation (19). The wall of the tube and the outer wall of the annulus are of uniform temperature, while the inner wall of the annulus is insulated (see Case 3A of Table 1). The data in Fig. 2 for the tube was obtained by interpolation between Hornbeck's Nusselt number curves for $Pr = 0.7$ and $Pr = 2.0$. The data in the figure for the annulus is $\overline{Nu}$ as defined by equation (38).

As another means of verification, the present model was used to obtain the fundamental Graetz solution of the second kind with the outer wall heated for the geometry ($\varepsilon = 0.5, \gamma = 0.4$). The resultant surface temperature distributions at the outer and inner walls, which can be found in Figs. 6.9 and 6.10, respectively, of [9], agree with the graphical data of [3].

For fundamental solutions of the second kind, $\bar{\theta}$ obtained from the numerical approximation of equation (32) can be verified with the exact $\bar{\theta}$ given by

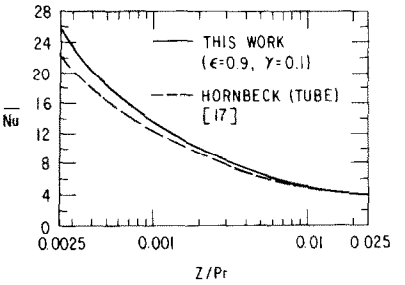

FIG. 2. Nusselt number comparison for $Pr = 1.0$. This work ($\varepsilon = 0.9, \gamma = 0.1$) vs the circular tube solution of Hornbeck [17].

either equation (33) or (34). Close agreement between numerically calculated and exact values of $\bar{\theta}$ was obtained in Graetz solutions for both the outer wall heated case and the inner wall heated case. Additional verification of the present thermal model and the hydrodynamic model of [10] was obtained by performing this $\bar{\theta}$ comparison for $Pr = 1.0$. A fundamental solution of the second kind with the inner wall heated was obtained for the geometry ($\varepsilon = 0.7$, $\gamma = 0.3$). Table 3, which characterizes the thermal entrance region for this case, provides a comparison between $\bar{\theta}$ of equation (32) and $\bar{\theta}_{2B}$ of equation (34). At small values of Z/Pr, such as 0.01, small differences between small values of $\bar{\theta}$ and $\bar{\theta}_{2B}$ produce large fractional errors. At higher values of Z/Pr, however, only very small fractional errors are observed. For example, at $Z/Pr = 0.1$ and 1.0 the fractional errors of $\bar{\theta}$ of equation (32) are only 0.69% and -0.13%, respectively.

The effects of eccentricity and the influence of Prandtl number were studied for the geometry ($\varepsilon = 0.5$, $\gamma = 0.5$). Since [3] has already solved the Graetz problem with heat flux boundary conditions, temperature boundary conditions given by Case 1B of Table 1 were chosen for the present study. The Graetz problem, $Pr = 1.0$, and $Pr = 0.05$ are considered.

The Prandtl number determines the relative sizes of the thermal and hydrodynamic entrance lengths. For $Pr = 1.0$, both entrance lengths are of the same order of magnitude. As $Pr \to \infty$, the thermal entrance length becomes much larger than the hydrodynamic one, and the Graetz problem is approached. The effect of very small values of Pr can best be understood by referring to equation (23). A very small Pr generally causes the left-hand side to be very small except at small values of Z where the quantity in the first set of parentheses is large. Hence, beyond these small values of Z, θ is fully developed while the flow is not. Because the Peclet number, i.e. $Re \cdot Pr$, must be at least 50 to preclude significant axial condition of heat, the value $Pr = 0.05$, which corresponds to liquid metals, was arbitrarily chosen as being representative of the minimum Pr for which the present analysis can be expected to produce accurate solutions.

The Graetz temperature and wall heat flux distributions of Figs. 3–5 dramatize the effects of eccentricity. While Fig. 3 shows the θ distribution across the duct at the narrowest and widest points of the annular gap, Figs. 4 and 5 respectively show the distribution of Φ_{iw} at the heated boundary and the distribution of Φ_{ow} at the unheated boundary. The arc length, Ω in the figures, is measured along either surface from the widest point of the annular gap to the narrowest. All three figures show that the narrowest point reaches fully developed thermal conditions much closer to the inlet than does the widest. Figures 4 and 5 show that for $Z/Pr = \infty$ the largest heat flux occurs at the narrowest point. This is as expected because when the temperature is fully developed all of the heat transfer is by conduction across the fluid from the inner wall to the outer. Figure 4 also shows that near the inlet the largest heat flux along the heated wall is at the widest point rather than at the narrowest. This occurs because convective heat transfer is very important near

Table 3. Fundamental solution of the second kind, inner wall heated, $\varepsilon = 0.7$, $\gamma = 0.3$, $Pr = 1.0$

Z/Pr	$\bar{\theta}_{2B}$*	$\bar{\theta}$†	$\theta_{max}^{+}{}^{\ddagger} - \bar{\theta}$	Nu_{iw}§	$\overline{Nu}_{iw}$¶
0.00001	0.000009	0.000014	0.01472	131.6	252.1
0.00002	0.000018	0.000029	0.02212	93.09	178.5
0.00006	0.000055	0.000091	0.03736	56.14	103.9
0.0001	0.000092	0.000155	0.04774	44.46	81.07
0.002	0.000185	0.000313	0.06597	32.96	58.83
0.0006	0.000554	0.000927	0.09932	21.40	36.02
0.001	0.000923	0.001520	0.1196	18.00	29.09
0.002	0.001846	0.002952	0.1490	14.85	22.46
0.006	0.005538	0.008040	0.1879	10.20	15.33
0.01	0.009231	0.01245	0.1991	7.859	12.54
0.02	0.01846	0.02225	0.2791	5.594	9.410
0.05	0.04615	0.04888	0.4830	3.963	6.471
0.1	0.09231	0.09295	0.6183	3.267	5.003
0.2	0.1846	0.1836	0.7094	2.841	4.004
0.374	0.3452	0.3439	0.7452	—	—
0.5	0.4615	0.4603	0.7505	2.647	3.221
1.0	0.9231	0.9219	0.7524	2.637	2.930
1.544	1.425	1.424	0.7528	2.637	2.827

* See equation (34).
† See equation (32).
‡ Maximum θ in Z plane.
§ See Table 2 and equation (39).
¶ See equation (40).

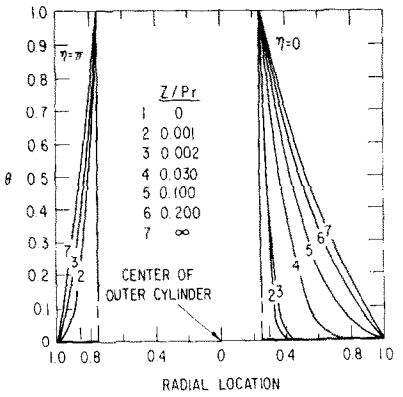

FIG. 3. Local dimensionless temperature in the plane of symmetry. Graetz, Case 1B, $\varepsilon = 0.5$, $\gamma = 0.5$.

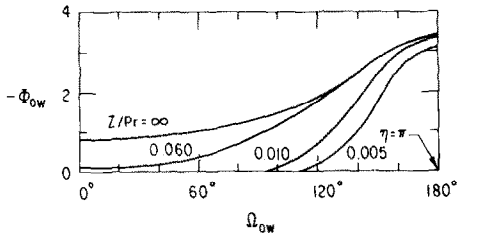

FIG. 5. Local dimensionless heat flux at the outer wall. Graetz, Case 1B, $\varepsilon = 0.5$, $\gamma = 0.5$.

the inlet and the fully developed flow velocities are largest at the widest point. This heat flux trend was not observed near the inlet in the $Pr = 1.0$ solution because in the developing flow solution the inlet velocity profile is uniform.

Figures 6 and 7 provide the axial distributions of $\bar{\Phi}_{iw}$ and $\bar{\Phi}_{ow}$ which are defined in an analogous manner to their $\overline{Nu}$ counterparts of equations (39) and (38), respectively. In the $Pr = 0.05$ analysis, the temperature solution became numerically unstable at $Z/Pr = 0.074$. Hence, beyond that point all $Pr = 0.05$ curves are approximated with a dashed line. The $Pr = \infty$ solution was obtained from equation (28) while the finite Pr solutions were obtained from equation (23). Since in the $Pr = 1.0$ solution, $Z = Z/Pr$, the two equations are the same except for the presence of the two transverse velocity terms in equation (23). Because the transverse flow near a wall is always directed away from the wall, the transverse flow tends to enhance the heat flux entering through the heated wall and to diminish the heat flux leaving through the unheated wall. Therefore, the $Pr = 1.0$ curve is above the $Pr = \infty$ curve in Fig. 6 and below the $Pr = \infty$ curve in Fig. 7. When the incoming heat flux is enhanced and the exiting heat flux is diminished, the average fluid temperature is enhanced and hence, in Fig. 8 the $Pr = 1.0$ curve is above the $Pr = \infty$ curve.

The axial distributions of $\overline{Nu}_{ow}$ and $\overline{Nu}_{iw}$ for parametric values of Pr, Fig. 9, provide the somewhat unexpected observation that all three $\overline{Nu}_{ow}$ curves have a relative maximum while all three $\overline{Nu}_{iw}$ curves have a relative minimum. This phenomenon is a product of eccentricity which is most pronounced in the Graetz solution at the outer wall. The thermal behavior of the entrance region may be visualized as a thermal boundary layer at the inner heated wall expanding toward the outer wall with increasing axial distance. Near the inlet Φ_{ow} and Nu_{ow} are essentially zero while $\bar{\theta}$ is increasing from its zero inlet value. Eccentricity enables the thermal boundary layer to contact the outer wall closer to the inlet than would otherwise be possible. Figure 5 shows, for example, that for the Graetz solution at $Z/Pr = 0.005$, while $-\Phi_{ow}$ is essentially zero over most of the outer circumference, it is close to its fully developed temperature value near the narrowest point of the annular gap. This non-zero portion of the $-\Phi_{ow}$ curve enables a sizable $-\bar{\Phi}_{ow}$ to occur in Fig. 7 at $Z/Pr = 0.005$, while Fig. 8 shows $\bar{\theta}$ at $Z/Pr = 0.005$ to still be rather small. Since, as indicated by Case 1B of Table 2, $\overline{Nu}_{ow}$ is $-\bar{\Phi}_{ow}/\bar{\theta}$, a rather sizable $\overline{Nu}_{ow}$ is seen in Fig. 9 at $Z/Pr = 0.005$ rather than the much smaller value of $\overline{Nu}_{ow}$ which would have occurred if the duct were concentric.

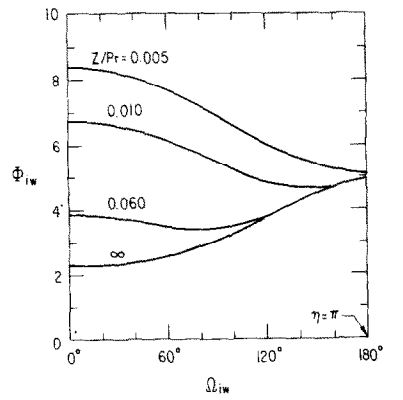

FIG. 4. Local dimensionless heat flux at the inner wall. Graetz, Case 1B, $\varepsilon = 0.5$, $\gamma = 0.5$.

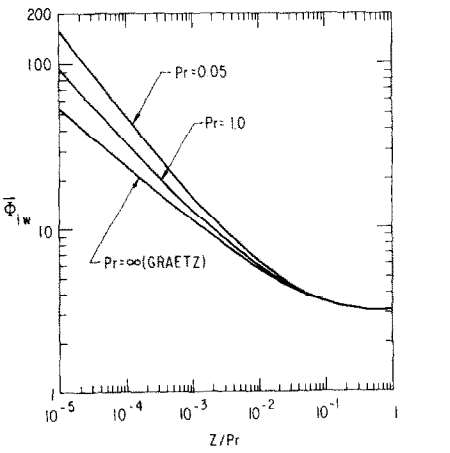

FIG. 6. Average dimensionless heat flux at the inner wall. Case 1B, $\varepsilon = 0.5$, $\gamma = 0.5$.

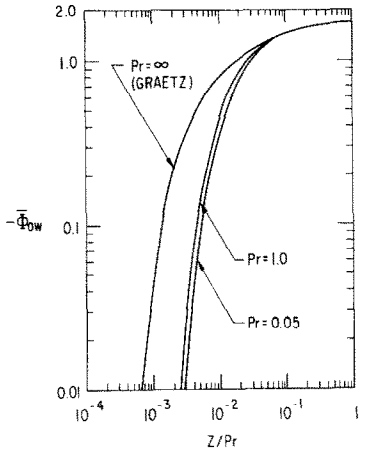

FIG. 7. Average dimensionless heat flux at the outer wall. Case 1B, $\varepsilon = 0.5$, $\gamma = 0.5$.

Since the Graetz solution has the largest values of $-\bar{\Phi}_{ow}$ in Fig. 7 and the smallest values of $\bar{\theta}$ in Fig. 8, it also has the largest values of $\overline{Nu}_{ow}$ in Fig. 9.

Table 4 provides values of thermal entrance length for the 17 thermal problems considered in [9]. The first set of three have already been discussed as part of the model verification and the next set of three were just described in the discussion of Figs. 3–9. The Graetz solution in the second set is also included in each of the remaining two sets, which contain Graetz solutions exclusively. The first set of Graetz solutions shows the effect of geometry on entrance length for fundamental solutions of the first kind with the inner wall heated. The three $\gamma = 0.5$ geometries in this set demonstrate the dramatic increase in entrance length with increasing eccentricity. The last set shows the effect of thermal boundary condition on entrance length for the geometry ($\varepsilon = 0.5, \gamma = 0.5$). In this set, the 1A and 1B cases have nearly equal entrance lengths as do the 2A and 2B cases. However, this is not true for the remaining two pairs of solutions. In [9], contour plots of $\theta - \bar{\theta}$ for Cases 2A and 2B show that for fully developed temperature, while the maximum θ, θ_{max}, occurs on the

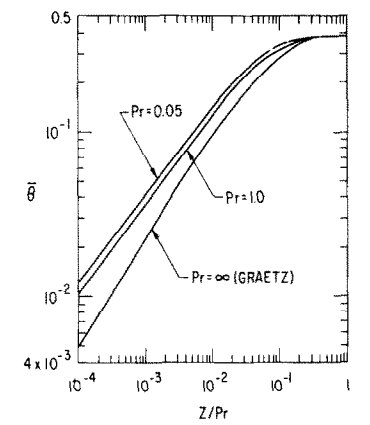

FIG. 8. Average dimensionless temperature. Case 1B, $\varepsilon = 0.5$, $\gamma = 0.5$.

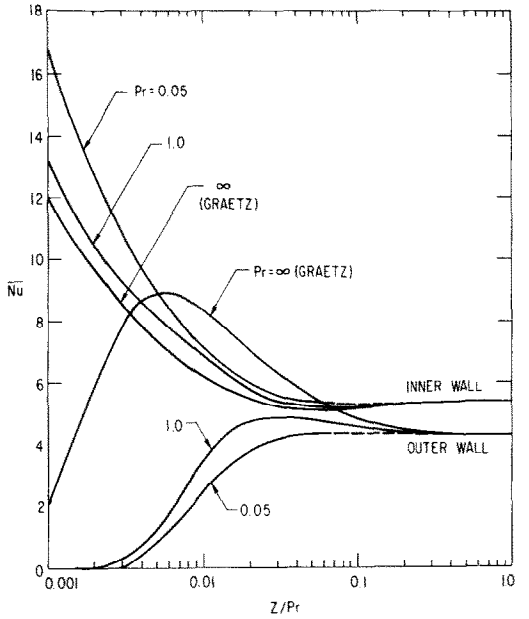

FIG. 9. Average Nusselt number. Case 1B, $\varepsilon = 0.5$, $\gamma = 0.5$.

heated boundary at the narrowest part of the annular gap, convection enables the minimum θ to occur at a distance from the insulated wall at the widest part of the gap.

Shah and London [11] have compiled thermal data in a form which is practical for use by designers of compact heat exchangers. As indicated by the reference, data generated by the current analysis was transmitted by private communication. Consequently, axial distributions of $\overline{Nu}$ and $\bar{\theta}$ or θ_{max} are tabulated in [11] for many of the cases listed in Table 4. Since the current nomenclature does not agree with that of [11], the Appendix compares essential variables of the two nomenclatures.

5. CONCLUSIONS

The hydrodynamic entrance region solution of [10] has enabled the thermal solution for the combined entrance region problem to be obtained. An axial distribution of $\overline{Nu}_{ow}$ for the eccentric geometry ($\varepsilon = 0.9, \gamma = 0.1$) and $Pr = 1.0$ compared reasonably well with a constant wall temperature solution published for the circular tube. Moreover, a Graetz solution for the geometry ($\varepsilon = 0.5$, $\gamma = 0.4$) and boundary conditions of the second kind was verified with a published solution.

Some of the salient aspects of the solution of the energy equation are: (1) the use of both variable axial step sizes and variable ζ intervals in the finite difference grid, (2) the use of Allen's method in the finite difference representation, and (3) the use of an implicit alternating-direction method.

While 17 thermal entrance region problems were considered, emphasis was placed on Case 1B of Table 1 for which the effects of eccentricity and Pr were studied for the geometry ($\varepsilon = 0.5$, $\gamma = 0.5$). This analysis

Table 4. Thermal entrance region problems

Geometry ε	Geometry γ	Fundamental solution (Case)*	Prandtl number	Thermal entrance length (Z/Pr)†
0.9	0.1	3A	1.0	0.400
0.5	0.4	2A	∞	0.675
0.7	0.3	2B	1.0	0.374
0.5	0.5	1B	∞	0.393
0.5	0.5	1B	1.0	0.356
0.5	0.5	1B	0.05	less than 0.356
0.5	0.9	1B	∞	0.433
0.9	0.5	1B	∞	0.575
0.5	0.5	1B	∞	0.393
0.1	0.5	1B	∞	0.175
0.5	0.1	1B	∞	0.302
0.5	0.5	1A	∞	0.390
0.5	0.5	1B	∞	0.393
0.5	0.5	2A	∞	1.10
0.5	0.5	2B	∞	1.15
0.5	0.5	3A	∞	0.785
0.5	0.5	3B	∞	1.46
0.5	0.5	4A	∞	1.31
0.5	0.5	4B	∞	0.821

* See Table 1.

† For fundamental solutions of the second kind the thermal entrance length is arbitrarily taken to be the value of Z/Pr at which the difference between the maximum θ and $\bar{\theta}$ is 99% of its fully developed temperature value. For the other three fundamental solutions the entrance length is arbitrarily taken to be the value of Z/Pr at which $\bar{\theta}$ is 99% of its fully developed temperature value.

demonstrated why eccentricity can cause an axial distribution of $\overline{Nu}$ to behave in a non-monotonic fashion.

In conclusion, the thermal behavior of the combined entrance region has been analyzed and a vehicle for providing additional thermal solutions for eccentric annuli has been provided.

REFERENCES

1. A. P. Hatton and A. Quarmby, Heat transfer in the thermal entry length with laminar flow in an annulus, *Int. J. Heat Mass Transfer* **5**, 973–980 (1962).
2. R. E. Lundberg, P. A. McCuen and W. C. Reynolds, Heat transfer in annular passages. Hydrodynamically developed laminar flow with arbitrarily prescribed temperatures or heat fluxes, *Int. J. Heat Mass Transfer* **6**, 495–529 (1963).
3. V. D. Vilenskii, Y. V. Mironov and V. P. Smirnov, Numerical solution of the problem of heat transfer in an annular channel, *High Temperature* **9**, 699–704 (1971).
4. K. C. Cheng and Guang-jyh Hwang, Laminar forced convection in eccentric annuli, *A.I.Ch.E. Jl* **14**, 510–512 (1968).
5. M. L. Trombetta, Laminar forced convection in eccentric annuli, *Int. J. Heat Mass Transfer* **14**, 1161–1173 (1971).
6. Katsuhisa Murakawa, Heat transfer in entry length of double pipes, *Int. J. Heat Mass Transfer* **2**, 240–251 (1961).
7. H. S. Heaton, W. C. Reynolds and W. M. Kays, Heat transfer in annular passages. Simultaneous development of velocity and temperature fields in laminar flow, *Int. J. Heat Mass Transfer* **7**, 763–781 (1964).
8. R. W. Shumway and D. M. McEligot, Heated laminar gas flow in annuli with temperature-dependent transport properties, *Nucl. Sci. Engng* **46**, 394–407 (1971).
9. E. E. Feldman, The numerical solution of the combined thermal and hydrodynamic entrance region of an eccentric annular duct. Ph.D. thesis, Carnegie-Mellon University, Pittsburgh, PA (1974).
10. E. E. Feldman, R. W. Hornbeck, and J. F. Osterle, A numerical solution of laminar developing flow in eccentric annular ducts. *Int. J. Heat Mass Transfer* **25**, 231–241 (1982).
11. R. K. Shah and A. L. London, *Laminar Flow Forced Convection in Ducts*. Academic Press, New York (1978).
12. W. F. Hughes and E. W. Gaylord, *Basic Equations of Engineering Science*. Schaum, New York (1964).
13. W. C. Reynolds, R. E. Lundberg and P. A. McCuen, Heat transfer in annular passages. General formulation of the problem for arbitrarily prescribed wall temperatures or heat fluxes, *Int. J. Heat Mass Transfer* **6**, 483–493 (1963).
14. Brice Carnahan, H. A. Luther and J. O. Wilkes, *Applied Numerical Methods*. John Wiley, New York (1969).
15. D. N. de G. Allen and R. V. Southwell, Relaxation methods applied to determine the motion, in two dimensions, of a viscous fluid past a fixed cylinder, *Q. J. Mech. appl. Math.* **8**, 129–145 (1955).
16. K. E. Torrance, Comparison of finite-difference computations of natural convection, *J. Res.* **72B**, 281–301 (1968).
17. R. W. Hornbeck, An all-numerical method for heat transfer in the inlet of a tube, ASME 65-WA/HT-36 (1965).

APPENDIX

Since Shah and London [11] on pp. 337–340 provide data generated by the current analysis, a nomenclature comparison is provided. While [11] uses a superscript $k = 1, 2, 3,$ or 4 enclosed in parentheses to indicate the fundamental solution type and a subscript $j = i$ or o to indicate inner or outer wall heated, the current nomenclautre generally relies on the text. The subscript l = i or o in [11], which indicates at which wall the dimensionless quantity is evaluated, corresponds to iw and ow, respectively, of the current nomenclature. Table A1 completes the comparison.

Table A1. Nomenclature comparison

Shah and London [11]	Current analysis
e^*	ε
$Nu_{x,lj}^{(k)}$	$\overline{Nu}_{i_w}$ or $\overline{Nu}_{i_w}$
r^*	γ
x^*	Z/Pr
$X_{lh,j}^{*(k)}$	value of Z/Pr corresponding to the thermal entrance length as defined in footnote † of Table 4
$\theta_{x,mj}^{(k)}$	$\bar{\theta}$
$\theta_{\max,j}$	maximum θ at a given value of Z

UNE SOLUTION NUMERIQUE DU CHAMP DE TEMPERATURE EN DEVELOPPEMENT POUR L'ECOULEMENT LAMINAIRE DANS DES CONDUITES ANNULAIRES EXCENTRIQUES

Résumé—L'équation d'énergie en coordonnées bipolaires est utilisée pour déterminer la distribution de température dans la région d'entrée thermique d'une conduite annulaire excentrique. La solution numérique s'appuie sur une méthode implicite à directions alternées. L'analyse de l'hydrodynamique dans la région d'entrée, nécessaire pour la solution thermique, est obtenue selon une méthode publiée par les auteurs. Une solution de Graetz déjà publiée pour une section annulaire excentrique et une solution hydrodynamique et thermique connue pour la région d'entrée de tubes circulaires sont utilisées pour vérifier la présente solution. On considère ici 17 combinaisons de conditions aux limites thermiques, de nombres de Prandtl, et de géométrie annulaire. La géométrie annulaire avec une excentricité relative et un rapport de rayons égaux à 0,5 est utilisée pour étudier les effets de l'excentricité et du nombre de Prandtl sur les distributions de température de fluide et de flux thermique à la paroi.

EINE NUMERISCHE LÖSUNG FÜR DEN TEMPERATURVERLAUF BEI LAMINARER ANLAUFSTRÖMUNG IN EXZENTRISCHEN RING KANÄLEN

Zusammenfassung—Die Energiegleichung in Bipolarkoordinatendarstellung wird zur Bestimmung der Temperaturverteilung im thermischen Anlaufgebiet eines exzentrischen ringförmigen Kanals herangezogen. Für die numerische Lösung wird ein implizites Verfahren der alternierenden Richtungen angewandt. Die Berechnung des hydrodynamischen Anlaufgebiets, welche die Geschwindigkeitsverteilungen liefert, die für die thermische Lösung benötigt werden, wurde aus einer veröffentlichten Lösung der oben genannten Autoren gewonnen. Eine veröffentlichte Graetz-Lösung für einen exzentrischen Ringraum und eine veröffentlichte Lösung für das gekoppelte thermische und hydrodynamische Anlaufgebiet für das Kreisrohr werden zur Überprüfung der vorliegenden Lösung verwendet. Diese Untersuchung behandelt 17 Kombinationen von fundamentalen thermischen Randbedingungen, Prandtl-Zahlen und Ringraumgeometrien. Die Ringraumgeometrie mit gleicher relativer Exzentrizität und einem Radienverhältnis von 0,5 wird zur Untersuchung der Einflüsse der Exzentriziät und der Prandtl-Zahl auf die Verteilungen von Fluidtemperatur und Oberflächenwärmestrom verwendet.

ЧИСЛЕННЫЙ РАСЧЕТ ИЗМЕНЕНИЯ ТЕМПЕРАТУРНОГО ПОЛЯ ПРИ НЕУСТАНОВИВШЕМСЯ ЛАМИНАРНОМ ТЕЧЕНИИ В ЭКСЦЕНТРИЧЕСКИХ КОЛЬЦЕВЫХ КАНАЛАХ

Аннотация — Для определения температурного поля на начальном тепловом участке эксцентрического кольцевого канала использовано уравнение энергии в биполярных координатах. Численное решение выполнено неявным методом переменных направлений. На основе ранее предложенного авторами решения проведен анализ гидродинамического начального участка с целью определения поля скоростей, необходимого для решения тепловой задачи. Полученные результаты проверены с помощью известного решения Гретца для эксцентрического канала, а также известного совместного решения для теплового и гидродинамического начальных участков круглой трубы. Проведен анализ 17 наборов основных тепловых граничных условий, значений числа Прандтля и кольцевой геометрии канала. Кольцевая геометрия с равным относительным эксцентриситетом и отношением радиусов, равным 0,5, используется для исследования влияния эксцентриситета и числа Прандтля на распределение температуры жидкости и плотности теплового потока на поверхности.